International Journal of GEOMATE, Nov., 2019 Vol.17, Issue 63, pp. 331 - 339
ISSN: 2186-2982 (P), 2186-2990 (O), Japan, DOI: https://doi.org/10.21660/2019.63.71127
Geotechnique, Construction Materials and Environment

SEEPAGE FAILURE IN FOUNDATION OF WEIR WITH CUT-OFF WALLS BY MODEL EXPERIMENTS AND ELASTO-PLASTIC FEM

* Kenji Okajima [1]

[1] Faculty of Bioresources, Mie University, Japan

*Corresponding Author, Received: 26 April 2019, Revised: 17 May 2019, Accepted: 01 June 2019

ABSTRACT: Two creep flow theories, Bligh's equation and Lane's equation, have been commonly used to determine the design criteria to prevent piping failure of the foundations of the weirs on soft ground. Scale-model experiments and finite element method (FEM) analysis were applied to test the reliability of these two methods. The scale-model experiments adopted six weir configurations in which creep length was held constant, but the number, position and length of the cut-off wall were altered. The critical difference in hydraulic head determined from the scale-model experiments was different for each weir configuration, despite the fact that a constant value would be produced by both creep flow theories. Whereas the creep flow theories were unable to represent this variation in critical head difference, FEM analysis predicted it well. The maximum shear strain contours produced by finite element analysis indicated that shear strain was concentrated in a similar domain to that which would be predicted by the Terzaghi's soil mass in the calculation of seepage failure of sheet piles. These results suggest that the Terzaghi's method is more accurate than the empirical creep flow theories for calculating critical head, provided the soil mass is defined correctly.

Keywords: Creep flow theories, The Terzaghi's method, Foundation of weir, Elasto-plastic FEM

1. INTRODUCTION

Creep flow is the slow percolation of water through the base and subsoil of weirs. The head loss of the creeping water is proportional to the length of travel, which has horizontal and vertical components, and sufficient head loss must be achieved to prevent forces occurring at the downstream end of the weir that cause piping action within the foundation. Based on a large set of case studies, Bligh's creep flow theory was developed as an empirical equation for the design of the floating weirs resting on a permeable layer (Bligh [1]); its purpose was to define the creep flow length required to prevent piping. Subsequently, the vertical component of creep length was found to reduce the danger of piping more than the horizontal component. Lane [2] thus suggested a weighted creep flow theory. Both creep flow theories are based on the assumption that piping is caused by the hydraulic gradient along the contact surface between the foundation and the weir. Cutoff walls under the weir and the length of the weir were adopted to promote the rapid reduction of the hydraulic gradient. After these studies, there are few basic studies on seepage failure of the foundation of the weir, and there are many studies on the safety of individual weirs (e.g. Khassaf et al.[3], Kaini et al.[4]). Oh and Woo[5] analyzed seepage failure under the weir without cut-off walls by ABAQUS. However, the effectiveness of ABAQUS to analyze seepage failure was not verified. The effectiveness of the elasto-plastic FEM on the seepage failure of the weir without cut-off walls has been confirmed by Okajima et al.[6].

The purpose of this study was, therefore, to scrutinize the traditional Bligh and Lane creep flow methods of determining practical design criteria for weirs with cut-off walls and to clarify the mechanisms for seepage failure under weirs with cut-off walls by means of physical scale-model experiments and elasto-plastic modeling using the finite element method (FEM). These studies were started by Okajima et al.[7] In this study, cases were increased and examined in more detail. A series of scale-model experiments and compared the results with the design criteria suggested by the Lane and Bligh methods were conducted. The seepage failure mechanism by applying elasto-plastic FEM to the experimental conditions and then compared the results with those that would be achieved by the Terzaghi's soil mass method (Terzaghi and Peck, [8]) also was estimated.

2. CREEP FLOW THEORIES

To prevent piping at the downstream side of weirs on soft ground, a safe creep length has to be ensured along the undersurface and sides of the weir. Two empirical methods for determining the minimum creep length were developed. Bligh's method defines the design criterion for creep length as

$$L_B \geq C_B \Delta H \quad (1)$$

Where L_B is Bligh's creep length, the seepage length measured along the undersurface and sides of a weir on soft ground, C_B is Bligh's creep ratio which varies depending on the ground characteristics and ΔH is the difference in hydraulic head between the upstream and downstream sides of the weir. In fine sand, C_B is 15. The critical head difference is ΔH_{CB} which is the head difference above which piping failure begins, occurs when $L_B = C_B \Delta H_{CB}$.

Lane's method defines the design criterion for creep length as:

$$L_L \geq C_L \Delta H \tag{2}$$

Where L_L is the weighted creep length?

$$L_L = \sum l_v + k_v / k_h \sum l_h \tag{3}$$

Where l_v is the seepage length of vertical direction (angle of incline more than 45°), l_h is the seepage length in the horizontal direction (angle of incline less than 45°). k_v is the vertical coefficient of permeability and k_v is the horizontal coefficient of permeability. By convention, a value of 1/3 has been used for k_v / k_h. Lane's creep ratio C_L varies depending on the characteristics of the ground. In fine sand, C_L is 7.0. The critical head difference is ΔH_{CL}, occurs when $L_L = C_L \Delta H_{CL}$.

3. SCALE MODEL EXPERIMENTS

The experimental scale models were constructed in a glass-walled sand box 1000 mm long, 200 mm wide and 500 mm high. The weirs were fixed to the side glass walls in the experiments. Permeable soil layers were prepared using poorly graded clean Toyoura sand (Table 1). The dry sand was poured from a hopper into 5 mm of free water for every 10 mm of the sand layer. A reproducible high bulk density was obtained in the sand layers by this method: the relative density was about 85%. The weir was made of rigid acrylic plates. The bottom and sides of the weir were lined with sandpaper to create friction between the sand layer and the weir to prevent roofing which is the piping that occurs on the boundary of the weir and the sand layer. The weir was fitted with a cut-off wall made of aluminum plate. The weir was fixed to the sand box by silicone adhesive and the joins between the weir and the sand box were sealed with silicone sealant (Fig. 1). The sand layer was 150 mm high.

The water levels on the upstream and downstream sides of the weir were first set equal, and then the downstream water level was lowered incrementally (5 mm each hour). As the head difference increased, seepage flowed beneath the weir was observed. The vertical displacement of the top of the sand layer at 30mm downstream from the weir was measured by the laser distance meter. When piping or boiling was first observed, the critical head difference was deemed to have been reached. At that time the uptrend of the coefficient of permeability was observed each time.

A series of scale-model experiments and elasto-plastic FEM was conducted using 16 different weir configurations (Fig. 2). All weir configurations had the same creep length, 180 mm for Bligh's creep length and 123 mm for Lane's creep length. In Fig. 2, model experiments and elasto-plastic FEM were conducted on the 7 weirs with the asterisk (*). Only elasto-plastic FEM was conducted on the 7 weirs without the asterisk (*). The weirs in model experiments were fixed to the side glass walls and did not move during the experiments. The experiments were conducted with three replicates for weirs 1 to 6 and two replicates for weir 7.

The weirs were divided into three groups according to the depth of the weir, the position of the cut-off wall, and the positioning of two cut-off walls (Fig. 2).

In the depth group, the penetration depth of the weir was 0 mm for weir 0, 10 mm for weir 1, 20 mm for weir 2, and 50 mm for weir 3. The total weir plus cutoff wall depth was 50 mm in each case (i.e., for weir 3 there was no cutoff wall).

Table 1 Properties of the Toyoura sand

Sand properties	Unit	Toyoura sand
Mean particle diameter	mm	0.17
Uniformity coefficient		1.46
Maximum density	g/cm^3	1.65
Minimum density	g/cm^3	1.36
Specific gravity		2.65

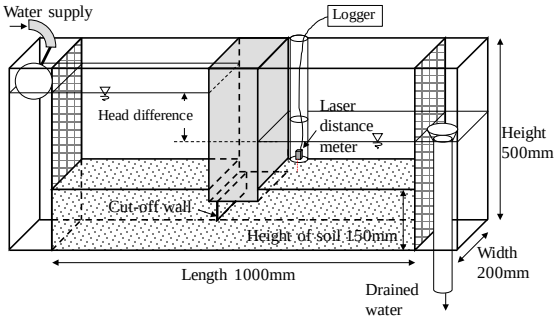

Fig. 1 Layout of the model experiment apparatus

In the position group 1, a weir penetration depth of 10 mm and cutoff wall depth of 40 mm was used for each weir, but the cutoff wall position was changed: 5 mm from the "upstream" end of the weir (weir 4), the mid-position of the weir (the same as weir 1), 20 mm from the "downstream" end of the weir (weir 8), 5 mm from the "downstream" end of the weir (weir 5) and the "downstream" end of the weir (weir 9).

In the other position group 2, the weir penetration depth of 20 mm and cutoff wall depth of 30 mm was used for each weir, but the cutoff wall position was changed: 5 mm from the "upstream" end of the weir (weir 10), the mid-position of the weir (the same as weir 2), 20 mm from the "downstream" end of the weir (weir 11), 5 mm from the "downstream" end of the weir (weir 12) and the "downstream" end of the weir (weir 13).

In the third group, called the "two cutoff wall group", two cutoff walls of different length were provided, one 30 mm and one 10 mm or one 20 mm and one 20 mm, each being positioned 5 mm from either end of the weir. In weir 6, the 30 mm cutoff was placed at the upstream end. In weir 14, the 20 mm cutoff was placed at both ends. In weir 7 the 30 mm cutoff was placed at the downstream end.

4. SEEPAGE ANALYSES AND ELASTO-PLASTIC FEM

In this study, the finite element analysis consisted of two steps. The first step was the seepage flow analysis by FEM. The second was seepage failure analysis by elasto-plastic FEM based on infinitesimal deformation condition, in which the seepage forces as the external force were input to all nodes of the ground. When piping or boiling was first observed, the uptrend of the coefficient of permeability was observed each time. In this model experiment, it was thought that the uniformity of the ground was maintained until piping and boiling occurred. Therefore, the seepage force as the external force increases in proportion to the head difference, but the seepage and stress analysis were not coupled in the elasto-plastic FEM. This model has been verified in the seepage failure of sheet piles (Okajima et al.[9]).

4.1 Constitutive Model of the Elasto-plastic Model

The finite element analysis employs the elasto-plastic constitutive equations with a non-associated flow rule and strain hardening-softening. The constitutive equations based on the yield function of the Mohr-Coulomb and the plastic potential function of the Drucker-Prager. The finite element is a 4-noded iso-parametric element with one point integration. The explicit dynamic relaxation method combined with the generalized return-mapping algorithm is applied. The elasto-plastic constitutive relations including the effect of the shear band are employed. Initial stress was calculated as the product of unit volume weight and ground depth, assuming horizontal ground. The earth pressure coefficient K_0 was 0.6 as ca onstant value.

A simplified and generalized version of mesh size-dependent softening modulus method (Tanaka and Kawamoto[10]) is used in this study. A material model for a real granular material (i.e., Toyoura sand) with a high angle of internal friction is used with the features of nonlinear pre-peak, pressure-sensitivity of the deformation and strength characteristics of sand, non-associated flow characteristics, post-peak strain softening, and strain-localization into a shear band with a specific width (Tatsuoka et al.[11]; Siddiquee et al. [12]). The material model will be briefly described in this section.

The yield function (f) and the plastic potential function (Φ) are given by

$$f = \alpha I_1 + \frac{\bar{\sigma}}{g(\theta_L)} = 0 \tag{4}$$

$$\Phi = \alpha' I_1 + \bar{\sigma} = 0 \tag{5}$$

Where

$$\alpha = \frac{2\sin\phi}{\sqrt{3}(3-\sin\phi)} \tag{6}$$

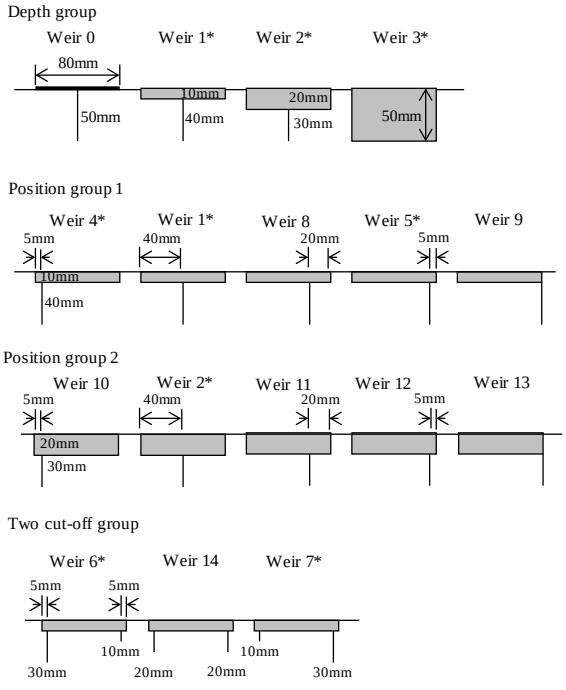

Fig. 2 Three types of group of scale-model experiments (*) and FEM

$$\alpha' = \frac{2\sin\psi}{\sqrt{3}(3-\sin\psi)} \tag{7}$$

Where I_1 is the first invariant (positive in tension) of deviatoric stresses and $\bar{\sigma}$ is the second invariant of deviatoric stress. With the Mohr-Coulomb model, $g(\theta_L)$ takes the following form.

$$g(\theta_L) = \frac{3-\sin\phi}{2\sqrt{3}\cos\theta_L - 2\sin\theta_L\sin\phi} \tag{8}$$

ϕ is the mobilized friction angle and θ_L is the Lode angle. The frictional hardening-softening functions expressed as follows are used.

Hardening-regime:

$$\alpha(\kappa) = \left(\frac{2\sqrt{\kappa\varepsilon_f}}{\kappa+\varepsilon_f}\right)^m \alpha_p \tag{9}$$

Softening-regime:

$$\alpha(\kappa) = \alpha_r + (\alpha_p - \alpha_r)\exp\left\{-\left(\frac{\kappa-\varepsilon_f}{\varepsilon_r}\right)^2\right\} \tag{10}$$

Where m, ε_f and ε_r are the material constants and α_p and α_r are the values of α at the peak and residual friction angle.

Shear banding was introduced in the numerical analysis through a strain localization parameter (Tanaka and Kawamoto[10]) in the following additive decomposition of total strain increment:

$$d\varepsilon_{ij} = d\varepsilon_{ij}^e + s\,d\varepsilon_{ij}^p \quad , \quad s = F_b / F_e \tag{11}$$

Where F_b is the area of a single shear band in each element; and F_e is the area of the element.

The elastic model depends on the mean stress and is given by the following formula. $\boldsymbol{\kappa}$ is the parameter of plastic strain.

$$\square = \square_0 \frac{(2.17-\square)^2}{1+\square}\square^{1/2} \qquad (\square \geq \square\square\ \square\square/\square^{\square}) \tag{12}$$

$$\square = \square_0 \frac{(2.17-\square)^2}{1+\square}\sigma_{\square} \qquad (\square < \square\square\ \square\square/\square^{\square}) \tag{13}$$

$$\square = \frac{2(1+\nu)\square}{3(1-2\nu)\square} \tag{14}$$

Where $\square$ is the shear modulus, $\square$ is the bulk modulus, e is the void ratio, ν is Poisson's ratio. $\square_0$ is the material constant.

4.2 Input Parameter and FEM Mesh

In the elasto-plastic finite element analysis, the material constants of Toyoura sand are as follow relative density = 88%, void ratio e=0.64, Poisson's ratio ν=0.3, residual friction angle (ϕ_r)= 33 degree. The calibration of the other elasto-plastic parameter of air-dried Toyoura sand in the elasto-plastic constitutive model was performed using the plane strain compression tests by Tatsuoka et al (1993). m = 0.3, ε_f = 0.1, ε_r = 0.6 and shear band thickness is 3mm. The material constant $\square_0$ is 40,000 kN/m^2.

The analysis was performed using a series of finite element meshes corresponding to each scale-model experiment (Fig. 3). The weirs were fixed to the side glass walls in the experiments. The mesh of the weirs and cut-off part had been removed. Elements bordering on the weir were boundary elements, in which the friction was set equal to the friction between sand and weir (ϕ=10 degree).

5. RESULT AND DISCUSSION

5.1 Results of Model Experiments

The results of the scale-model experiments are shown in Table 2. The relative density was about 85% and ranged from 81.2% to 88.9%. Piping was observed in some of the model configurations. Heaving was observed when the sand deformed on the downstream side. The critical head differences were similar between the replicates of each configuration, demonstrating a high level of reproducibility.

Large variation was observed in the critical head difference of the different model configurations, despite all having the same creep length and therefore the same value of critical head difference as calculated by Bligh's and Lane's creep flow theories. This result shows that the creep flow theories did not reliably predict the critical head difference.

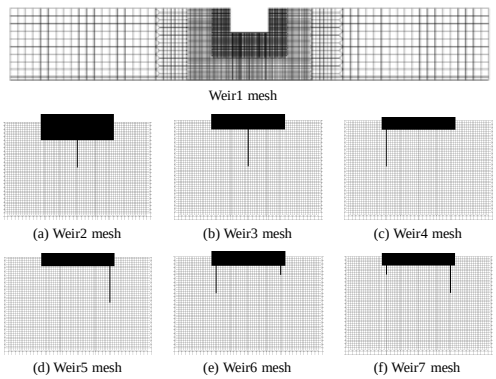

Fig. 3 Finite element meshes corresponding to each scale-model experiment

5.2 Critical Head Difference

The result of the scale-model experiments and FEM analyses of each of the weir groups are discussed with reference to the effectiveness of FEM and the observed seepage failure of the foundations of the weirs. All configurations had the same Bligh's creep length of 180 mm and Lane's creep length of 123 mm.

In the position group 1 of a weir penetration depth of 10 mm and cutoff wall depth of 40 mm (weirs 4, 1, 8, 5 and 9), the critical head difference gradually increased as the cutoff wall was moved towards the downstream end of the weir (Fig. 4). The FEM analysis predicted the observed critical head difference well. The critical head difference from Bligh's creep length corresponded with the observed and FEM value for weir 5 and FEM value for weir 9, where the cutoff wall was at the downstream end of the weir. Lane's creep length predicted the FEM value of the critical head difference when the cutoff wall was approached to the upstream end of the weir. In the position group 2 of a weir penetration depth of 20 mm and cutoff wall depth of 30 mm (weirs 10, 2, 11, 12 and 13), the critical head difference gradually increased similar Fig. 4 as the cutoff wall was moved towards the downstream end of the weir (Fig. 5). In Fig. 4 and Fig. 5, when the cut-off wall was located at the downstream end of the weir, the FEM value of the critical head differences of weir 5, 9, 12 and 13 were same regardless of the weir penetration depth. The FEM value of the critical head difference in Fig.5 was larger than them in Fig. 4 when the cutoff wall was moved towards the upstream end of the weir.

Table2 Soil properties and critical head difference of scale model experiments

Pattern	Relative density %	Critical head differenece mm	Piping / Boiling	Average of critical water head mm
Weir1	82	80	Piping	87
	86.3	90	Piping	
	83.6	90	Piping	
Weir2	84.7	140	Piping	137
	86.1	145	Boiling	
	84.5	125	Piping	
Weir3	88.9	250	Boiling	258
	85.1	251	Boiling	
	81.4	271	Boiling	
Weir4	87.4	70	Piping	73
	81.2	75	Piping	
	81.5	75	Piping	
Weir5	82.6	155	Boiling	170
	83.1	175	Boiling	
	87.4	180	Boiling	
Weir6	86.6	130	Piping	133
	84.5	135	Piping	
	82.6	135	Piping	
Weir7	83.6	145	Boiling	155
	82.3	165	Boiling	

In the depth group (weirs 0, 1, 2, and 3), the critical head difference gradually increased as the penetration depth of the weir increased (Fig. 6). As in the position group, the predicted critical head difference from FEM analysis corresponded closely to the observed values. The critical head difference from Bligh's creep length did not correspond with any of the observed or FEM-predicted values, but that from Lane's creep length corresponded with the observed and FEM-predicted value of weir 2 (20 mm penetration).

In the two cutoff wall group (weirs 6, 14 and 7), the critical head difference was only slightly altered by reversing the position of the longer and shorter cutoff walls (Fig. 7). The critical head difference was slightly greater in weir 14 where the same length cutoff wall was set than weir 6. The critical head difference was greater in weir 7, where the longer cutoff wall was set at the downstream side. However, the critical head difference of weir 7 was still less than that of weir 5, which had one cutoff wall at the downstream side, although in weir 5 the single cutoff wall was 40 mm versus 30 mm for the longer wall in the two cutoff wall weirs. The results of FEM analysis again predicted the observed critical head differences well.

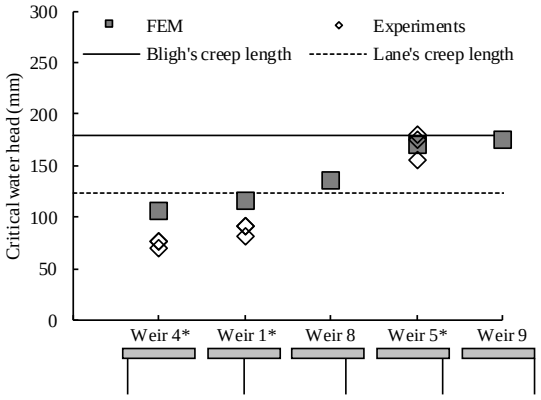

Fig. 4 Critical head difference of scale model experiments and FEM of Position group 1

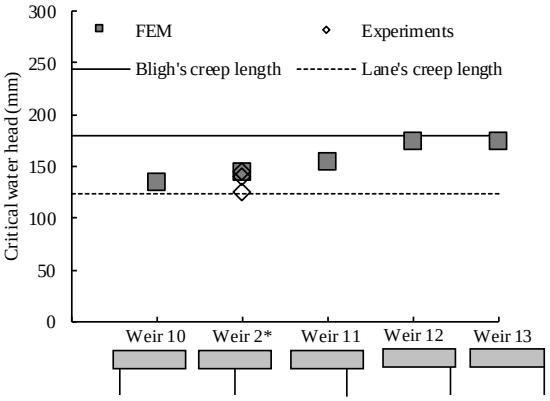

Fig. 5 Critical head difference of scale model experiments and FEM of Position group 2

For the weirs in which the penetration depth of the weir was 10 mm and the cutoff, wall was set at the upstream side or middle of the weir, FEM analysis computed higher values of a critical head difference than was observed in the scale-model experiments (weirs 1 and 4). This result indicates that the continuum model might not hold true when the number of sand particles at the downstream edge of the weir was about 62.5 (the average particle size was 0.16 mm). For the weir in which the penetration depth was 50 mm (weir 3), FEM analysis computed a lower critical head difference than the results of the scale-model experiment. This result suggests that the friction of the side glass wall caused the head difference to induce boiling of a large sand mass. These comparisons show that FEM analysis can reliably compute the critical head difference, whereas Bligh's and Lane's creep length theories offer a very low degree of certainty.

5.3 Vertical Displacement of the Surface

The vertical displacement of the surface of the sand layer at 30mm downstream from the weir was measured by the laser distance meter. The vertical displacement of the surface of the sand layer was the largest downstream in contact with the weir. However, deformation of the surface of the sand layer in contact with the weir occurred locally by piping. In this study, the surface of the sand layer slightly away from the weir was measured to evaluate the deformation of the whole sand layer. Measurements of the vertical displacement were conducted in all model experiments. The tendency for vertical displacement was almost the same in all model experiments.

Observed values and the elasto-plastic FEM values of the vertical displacement of two cut-off wall group were compared (Fig. 8). The surface of the sand layer slightly sank until just before the failure as the critical head difference gradually increased. Meanwhile, the surface of the sand layer continued to rise in some experiments as the critical head difference gradually increased. The elasto-plastic FEM values of the vertical displacement hardly increased until just before the failure. The displacement progressed rapidly when it reached the critical head deference. Finite element analysis could not predict subsidence of the sand layer well as the critical head difference gradually increased.

5.4 Maximum Shear Strain

The elasto-plastic FEM analysis contained frictional hardening–softening functions. When the maximum shear strain reached 0.1, the constitutive model changed from a hardening regime to a softening regime. At that time the shear band was considered to develop. Fig. 9 indicates the observed seepage failure area (red broken line) in the scale-model experiments of weir 4 at a head difference of 180 mm over critical head difference and the maximum shear strain distribution computed by FEM at a head difference of 110 mm.

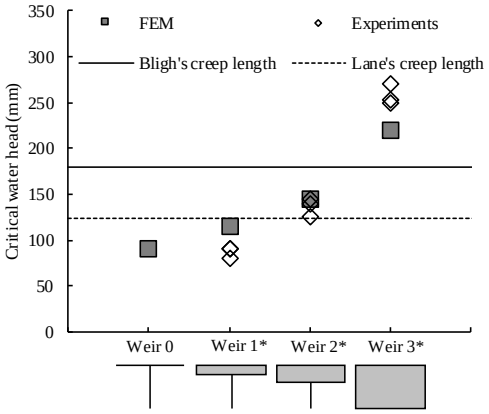

Fig. 6 Critical head difference of scale model experiments and FEM of Depth group

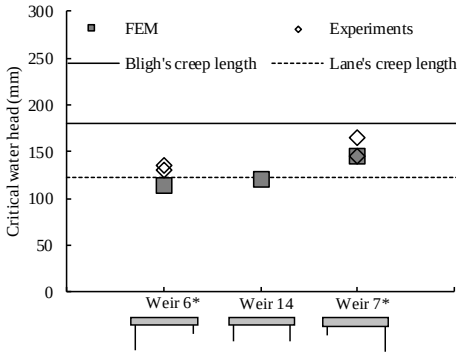

Fig. 7 The critical head difference of scale model experiments and FEM of two cut-off group

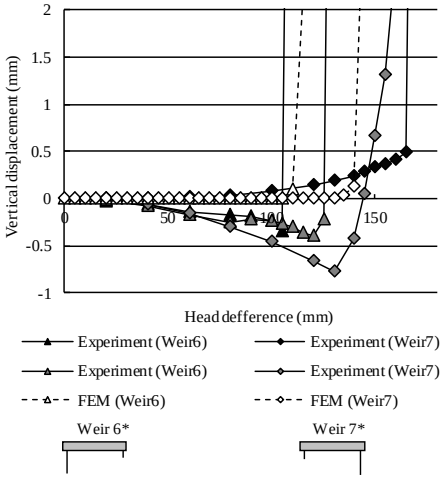

Fig. 8 Vertical displacement of Two cut-off group

When the failure area was compared with the region of concentration of maximum shear strain, it was clear that the FEM predicted the position and tilt of the shear band well. This result indicated that the FEM was able to predict the sand deformation by seepage failure.

5.5 Application of the Terzaghi's Method

To apply the Terzaghi's method to the seepage failure problem in weirs, we had to determine the soil mass area for the Terzaghi's method, first requiring the shape of the soil mass and second the penetration depth D of the soil mass with the cutoff wall set on the downstream side. The original size of the soil mass was $D*D/2$. We called this shape T1. The shape of the area of concentration of maximum shear strain from the elasto-plastic FEM was a trapezoid.We applied the Terzaghi's method for a trapezoidal soil mass (T2). The area of concentration of maximum shear strain from the elasto-plastic FEM was larger than the original size. We applied the Terzaghi's method for a soil mass of dimensions $D*3D/4$ (T3). The critical head differences obtained from these shapes of soil mass with the Terzaghi's method were compared with the critical head differences obtained from FEM in the position group of weirs. Fig. 9 shows the relationship between the three soil mass shapes and critical head difference. There were few differences in the critical head difference in each weir model. The critical head difference obtained by applying the original soil mass size with the Terzaghi's method was validated.

The original penetration depth D for use with the Terzaghi's method was the penetration depth of the cutoff wall. However, when the cutoff wall was set at close to the downstream end of the weir (Fig.10), the concentration of maximum shear strain appeared in the deep area from the end of the cutoff wall and shallow area from the downstream end of the weir. In this case, the penetration depth of the Terzaghi's method was regarded as the penetration depth of the weir (Soil 1) or the penetration depth of the weir plus cutoff wall (Soil 2). Fig. 10 shows the maximum shear strain contours for weir 5 and the areas of soil mass for Soil 1 and Soil 2. The critical head differences calculated with each soil mass were 153 mm for Soil 1 and 152 mm for Soil 2. There were few differences in critical head difference for each penetration depth. This showed that the Terzaghi's method was valid for determining the critical head difference for the downstream edge of weirs.

In this study, we considered that the penetration depth D was the depth of the downstream edge of the weir. Fig. 11 shows the results of applying the Terzaghi's method to the calculation of critical head for the scale-model weirs of the position group (Fig. 11(a)(b)), the depth group (Fig. 11(c)) and two cut-off group (Fig. 11(d)). The Terzaghi's method accurately predicted the critical head in both the position group and the depth group and was more accurate than creep theory at calculating variation in critical head in the seepage failure of weirs.

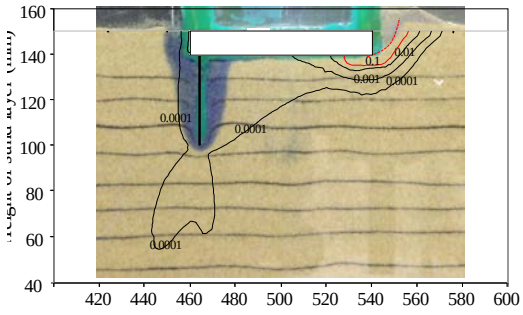

Fig. 8 Failure area in model experiment at head difference 180mm and maximum shear strain distribution at head difference 110mm of weir 4

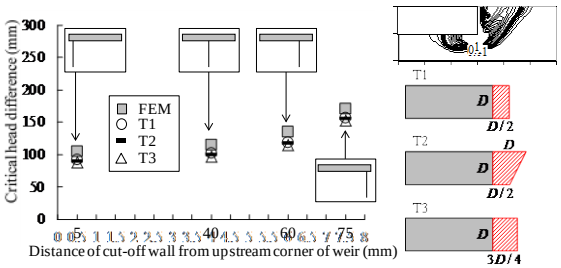

Fig. 9 Relationship between three types of shapes of soil mass and critical head difference

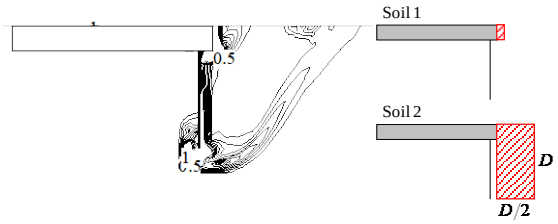

Fig. 10 Maximum shear strain contour line of Weir5 and areas of soil mass in Soil 1 and Soil 2

5. CONCLUSION

In this study, the traditional Bligh and Lane creep flow methods of determining practical design criteria for weirs with cut-off walls were scrutinize and the mechanisms for seepage failure under weirs with cut-off walls by means of physical scale-model experiments and elasto-plastic modeling using the finite element method (FEM) was clarified. Creep flow theories were reexamined by model six patterns experiments and finite element analyses that had the same creep length by changing the position and length of the cut-off wall in this study.

However, these critical head differences in model experiments were different from each pattern. The investigations show that Bligh's and Lane's creep flow theories are not reliable methods for predicting the critical head difference of weirs.

The FEM predicted these critical head differences of model experiments with any cut-off walls well. Finite element analysis could not predict

subsidence of the sand layer well as the critical head difference gradually increased. Maximum shear strain contour line by the finite element analysis indicated that shear strain concentrated in similar soil mass as Terzaghi assumed in the seepage failure equation.

It was suggested that Terzaghi's method was more effective than the creep theory to calculate the critical head difference if the soil mass was defined properly. The penetration depth D for the soil mass was the penetration depth of the weir.

6. REFERENCES

[1] Bligh, W. G., The practical design of irrigation works, London Constable, 1910, pp. 162-205.

[2] Lane, E.W., Security from Under seepage Masonry Dams on Earth Foundations", Trans. ASCE, Vol.100, 1935, pp. 1234-1351.

[3] Khassaf, S. I., Al-Adili, A. Sh., and Rasheed, R. S., Seepage analysis underneath Diyala weir foundation, Proceeding of IWTC 13, 2009, pp. 301-310.

[4] Kaini, S., Hayde, L.G., Schultz, B. and Marence, M., Seepage analysis underneath the headwork of Chanda Mohana Irrigation Scheme, Sunsari, Nepal, Proceedings of National Irrigation Seminar on Micro to Megha: Irrigation for Prosperous Nepal, 2011, pp.13-14.

[5] Oh, H. J. and Woo,Y. J., Fragility Analysis of Weir Structure Subjected to Flooding Water Damage, World Academy of Science, Engineering and Technology International Journal of Civil and Environmental Engineering, 2018, Vol.12(1), pp.75-80.

[6] Okajima, K. and Tanaka, T., Evaluation of analyses of downstream piping of weirs by model experiments and elasto-plastic FEM, Proceeding of ICSE 4, 2008, pp. 460-467.

[7] Okajima, K., Magara, N. and Iida, T., Reexamination of Creep Theory in the Foundation of Weirs by Model Experiments and Elasto-Plastic FEM, Proceeding of ICSE 5, 2010, pp. 560-569.

[8] Terzaghi, K. Peck, R. B., Soil Mechanics in Engineering Practice, John Wiley and Sons, 1948, 218–233.

[9] Okajima, K., Tanaka T., Zhang S. and Komatsu T., Model experiments and elasto-plastic finite element analysis about seepage failure of sand behind fixed sheet pile, Transaction of the JSIDRE, 260, 2009, pp. 107-112.

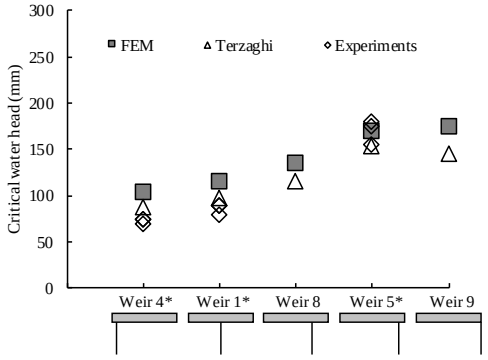

(a)The critical head difference of Position group 1

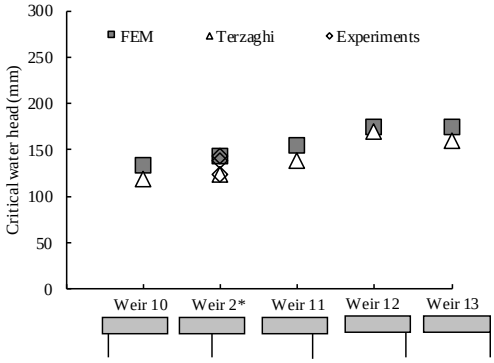

(b)The critical head difference of Position group 2

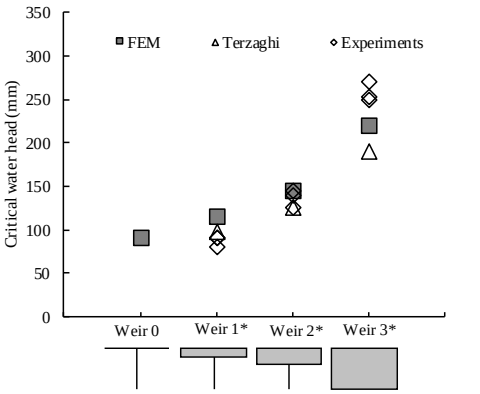

(c)The critical head difference of Depth group

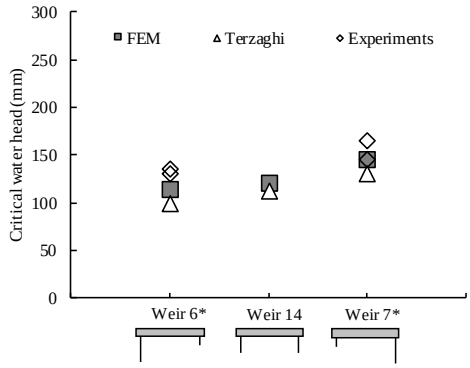

(d)The critical head difference of Two cut-off group

Fig. 11 The critical head difference in applying Terzaghi's method

[10] Tanaka, T. and Kawamoto, O., Three-dimensional finite element collapse analysis for foundations and slopes using dynamic relaxation, Proc. of Numer. Meth. in Geomech., 1988, pp. 1213-1218.

[11] Tatsuoka, F., Siddiquee, M. S. A, Park, C. S., Sakamoto, M. and Abe, F., Modeling Stress-Strain Relations of Sand, Soils and Foundations, Vol.33, Issue 2, 1993, pp. 60-81.

[12] Siddiquee, M.S.A., Tanaka, T., Tatsuoka F., Tani, K., Morimoto, T., Numerical simulation of bearing capacity characteristics of strip footing on the sand, Soils and Foundations, Vol.39, Issue 4, 1999, pp. 93-109.